Journal of Gerontology: BIOLOGICAL SCIENCES
2007, Vol. 62A, No. 4, 367–374

Telomere Dynamics in Macaques and Humans

Jeffrey P. Gardner,[1] Masayuki Kimura,[1] Weihang Chai,[2] Jameel F. Durrani,[1] Levon Tchakmakjian,[1] Xiaojian Cao,[1] Xiaobin Lu,[1] Guanghui Li,[1] Athanasios P. Peppas,[1] Joan Skurnick,[1] Woodring E. Wright,[2] Jerry W. Shay,[2] and Abraham Aviv[1]

[1]The Center of Human Development and Aging, Cell Biology and Molecular Medicine, Department of Preventive Medicine and Community Health, University of Medicine & Dentistry of New Jersey Medical School, Newark.
[2]Department of Cell Biology, University of Texas Southwestern Medical Center, Dallas.

In humans, telomere length in proliferating tissues shortens with age—a process accelerated with age-related diseases. Thus, telomere length and attrition with age in the nonhuman primate may serve as a useful paradigm for understanding telomere biology in humans. We examined telomere parameters in tissues of young and old *Macaca fascicularis* and compared them with several tissues from humans. Macaque telomeres were variable in length and exhibited partial synchrony (equivalence) within animals. They were longer than humans, partially because of longer subtelomeric segments. As skeletal muscle telomere length was unchanged with age, we used it as an internal reference to offset interanimal variation in telomere length. We identified age-dependent telomere attrition in lung, pancreas, skin, and thyroid. Similar to humans, telomerase activity was detected in spleen, thymus, digestive tract, and gonads. We conclude that factors that modify telomere attrition and aging in humans may also operate in the macaque.

TELOMERE dynamics (expressed by telomere length and attrition rate) is a record of the history of and the potential for replication of cultured somatic cells (1). It follows that if cellular replication is involved in organismal aging, telomere dynamics in proliferating tissues might provide insight into not only the biology of aging but also the pathology of age-related diseases. A body of epidemiological and clinical data suggests that relatively short telomeres and accelerated telomere attrition are linked to factors that define aging and diseases of aging in humans (2–12). But these studies hardly prove causality. Therefore, the discipline of gerontology would benefit from an animal model with the ability to define through experimental manipulations the relation between telomere dynamics and growth, development, and aging.

Telomerase knockout has been used to examine morbidity and aging in the mouse (13–15). However, the mouse is not as genetically close to humans as are nonhuman primates. In this context, several groups have characterized features of telomere biology in nonhuman primates (16,17). They showed that: (a) telomere length, measured by Southern analysis of the terminal restriction fragment length (TRFL), was longer in nonhuman primates than in humans (16); (b) the distribution of telomerase activity among tissues of nonhuman primates was quite similar to that of humans (16); and (c) critically shortened telomeres were associated with replicative impasse of cultured somatic cells of most nonhuman primates (17). In the present study, we thoroughly assessed telomere parameters and describe an approach that facilitates the tracking of telomere attrition in vivo in the nonhuman primate. For comparison, we have undertaken the same approach in several human tissues.

Materials and Methods

Macaque Tissues

Both captive and bred cynomolgus monkeys (*Macaca fascicularis*) were used as a source of tissues and internal organs. Ages of young (4–8 y) monkeys, bred in captivity, were based on date of birth. Older monkeys (17–23 y) that had been captured between ages 5–7 years (age estimated from general appearance, body weight, sexual development, and eruption of dentition) were kept in captivity for 12–17 years. Animals were housed in individual cages according to the guidelines of the Institutional Animal Care and Use Committee of the New Jersey Medical School. Tissues were obtained from 12 males (age range 3.6–21 y) and 11 females (age range 3.7–23 y) immediately following euthanasia. Tissues were cleaned of blood and adherent fat, rinsed in ice-cold physiological saline solution, and frozen at –80 °C. Since the exact age of the older monkeys was unknown, we stratified the animals into two categories: younger and older.

Human Tissues

Tissues from human lung, skin, and skeletal muscle were obtained from patients ($n = 11$, age range 50–76 y) who underwent pulmonary lobectomy for lung cancer. Surgical tissue samples were obtained from the skin at the incision site, the serratus posterior muscle, and the removed lobe of the lung. Careful attention was made to obtain normal lung samples from a site peripheral to the cancerous lesion to avoid the possibility that the samples contained microscopic extensions of the cancer. To further ascertain the absence of cancer from lung tissues, we measured telomerase activity in the samples. All samples were negative for telomerase.

Tissue donors signed an informed consent approved by the Institutional Review Board of the New Jersey Medical School. In addition, skin and lung tissue were obtained from autopsies, no later than 10 hours after death ($n = 12$, age range = birth–76 y). Kidney tissues (inner medulla, $n = 32$, age range = 0.1–71.4 y) from human subjects deceased by accidental causes were obtained from the Brain and Tissue Bank (BTB) for Developmental Disorders, University of Maryland, Baltimore.

DNA Isolation and Measurement of the Mean TRFL

Frozen tissues were pulverized in a liquid nitrogen-cooled mortar and DNA was isolated by phenol chloroform extraction. All DNA was assessed for integrity by electrophoresing 0.5 μg of DNA on 1% agarose gels and staining with Sybr Green I (Invitrogen, Carlsbad, CA). In some cases, TRFL was not measured due to low yields of DNA from tissue.

TRFLs were measured by Southern blot analysis (18) after electrophoresis of DNA on agarose gels. As TRFL is longer in macaques than in humans (16), we extended the resolution of the Southern analysis to accommodate longer telomeres. The 0.3% agarose gels provided better resolution of macaque telomeres than 0.5% gels, which are routinely used to resolve TRFLs in human DNA. TRFL analysis on macaque DNA was therefore performed on DNA electrophoresed on 0.3% agarose gels, and human DNA was resolved on 0.5% gels.

DNA samples were digested overnight with restriction enzymes *Hinf*I (0.5 U/μl) and *Rsa*I (0.5 U/μl) (Roche Diagnostics, Nutley, NJ). Eighteen DNA samples (~5 μg each) and 4 DNA ladders (1 kb and high mol wt DNA ladder [Invitrogen, monkey samples] or 1 kb mol wt ladder and λ DNA/*Hind*III fragments [Invitrogen, human samples]) were resolved on 0.3% or 0.5% agarose gels (20 cm × 20 cm) at 40 V (16 h). DNA was depurinated for 30 minutes in 0.25 N HCl, denatured 30 minutes in 0.5 mol/L NaOH/1.5 mol/L NaCl, and neutralized for 30 minutes in 0.5 mol/L Tris, pH 8/1.5 mol/L NaCl. The DNA was transferred for 1 hour to a positively charged nylon membrane (Roche Diagnostics) using a vacuum blotter. Membranes were hybridized at 65°C with the telomeric probe [digoxigenin 3′-end labeled 5′-$(CCCTAA)_3$] overnight in 5X SSC, 0.1% Sarkosyl, 0.02% SDS, and 1% blocking reagent (Roche Diagnostics). The membranes were washed three times at room temperature in 2X SSC, 0.1% SDS each for 15 minutes and once in 2X SSC for 15 minutes. Probe was detected by the digoxigenin luminescent detection procedure (Roche Diagnostics) and exposed on Hyperfilm XL (GE Healthcare, Piscataway, NJ).

TRFLs were determined by scanning each lane between 7 and 47 kb (monkey) or 3 and 22 kb (human) with a densitometer and comparing the scan with the closest reference molecular weight ladder (ImageQuant 3.11, GE Healthcare). The length of the mean TRFL (referred to as TRFL) was calculated as previously described (18) using the formula: $\text{mTRFL} = \Sigma\text{OD}(i)/\Sigma(\text{OD}(i)/\text{MW}(i))$, where OD($i$) is the optical density at a given position and MW(i) is the molecular mass at the same position. This formula accounts for the fact that longer telomeres bind more labeled probe and appear darker on the film. TRFL refers to the average TRFL for a sample run in duplicate on different gels.

Telomere Length Determined by Real-Time–Polymerase Chain Reaction (RT–PCR)

Telomere length in macaque tissues (biceps, liver, kidney medulla, skin, lung, and spleen) from 13 monkeys was measured using RT–PCR. DNA was diluted in 10 mmol/L Tris-HCl, 0.1 mmol/L EDTA, pH 7.5 (TE^{-4}) to 20 ng/μl and aliquotted to a 24-well PCR plate. DNA was denatured in a PE2400 thermal cycler (95°C for 30 min), followed by cooling to room temperature. RT–PCR to determine telomere (T) to single copy gene (S) ratios was performed as described by Cawthon (19) with several modifications. Telomere and single-copy gene PCRs used similar master mixes except for Mg^{2+} and oligonucleotide primer concentrations. Final concentrations of reagents in the PCR reaction were: 20 mmol/L Tris, 50 mmol/L KCl, 0.2 mmol/L dNTPs, 0.75 U Platinum Taq polymerase (Invitrogen), 0.4X Sybr Green 1, 1% DMSO, 2.5 mmol/L DTT, 40 ng *E. coli* DNA (MP Biomedicals, Irvine, CA), and 1.5 (T) or 3.5 (S) mmol/L $MgCl_2$. T RT–PCR contained 450 nmol/L of Tel1b (5′> 3′, CGG TTT GTT TGG GTT TGG GTT TGG GTT TGG GTT TGG GTT) and 450 nmol/L Tel2b (GGC TTG CCT TAC CCT TAC CCT TAC CCT TAC CCT TAC CCT) primers. S RT–PCR was performed for the nonhuman primate formyl peptide receptor single-copy gene *MMFPR1* (20). Reactions contained 450 nmol/L MMFPR1F (5′> 3′, CCT TTG TCG TAG CTG CCT TT) and 450 nmol/L MMFPR1R (GGC ACT TGT CGC ATC CAC T) primers. S RT–PCR was also performed for the *36B4* gene encoding acidic ribosomal phosphoprotein PO (19); the conditions for this PCR were identical to that of *MMFPR1*, except that each reaction contained 300 and 500 nmol/L (respectively) of 36B4U (5′> 3′, CAG CAA GTG GGA AGG TGT AAT CC) and 36B4D (CCC ATT CTA TCA TCA ACG GGT ACA A) primers. We verified *MMFPR1* gene copy number by comparing [MMFPR1] and [36B4] for each monkey sample; the ratio of [36B4]:[MMFPR1] was 0.99 ± 0.09 (mean ± *SD* [standard deviation] $n = 50$).

DNA samples (5 ng) were assayed in 20 μl final volume in 0.1 ml tubes for T and S RT–PCR on a Rotor-Gene 3000 (Corbett Research, Sydney, Australia). No Template Controls (NTC) and standard curves were run with each RT–PCR. DNA isolated from a single monkey liver was used as a reference DNA, and was diluted 2-fold (30 to 1.875 ng/tube) for each RT–PCR. Standards and NTC were assayed in duplicate and DNA samples were assayed in triplicate. Reaction mixtures were initially heated to 94°C for 1 minute followed by 22 (T) or 35 (S) cycles. Parameters for T RT–PCR cycles were 15 seconds at 95°C and 60 seconds at 58°C, and parameters for S RT–PCR cycles were 15 seconds at 95°C, 20 seconds at 58°C, and 20 seconds at 72°C. Fluorescence was acquired on the Sybr channel at the end of each cycle. Polyacrylamide gel electrophoresis analysis of PCR products and staining with Sybr Green I confirmed single-band products for *36B4* (74 bp) and *MMFPR1* (129 bp) RT–PCRs (data not shown). In addition, all RT–PCR experiments were followed by melt analysis

(72°C–99°C, 1°C/5 s ramp) and used to assess individual sample uniformity. Samples that showed secondary peaks or deviation by more than 1°C from their optimal melting point (86.5°C for *MMFPR1* and 84.4°C for *36B4*) were eliminated from subsequent analyses. C_t values, the threshold cycle at which amplicon fluorescence was significantly increased over background, was calculated using Rotor-Gene Analysis Software v4.94. Telomere and single-copy gene concentrations relative to each DNA reference standard curve were calculated, and relative T/S ratios for each sample were computed and averaged as previously described (19).

RT–PCR for human kidney DNA was performed as described above with the following modifications: 1) human placental DNA (Sigma) served as the reference DNA; 2) cycle parameters for T RT–PCR included 25 cycles at 95°C (15 s), 56°C (60 s); and 3) RT–PCR for *MMFPR1* was not performed.

The subtelomeric DNA segment of the TRFL is composed of DNA nucleotides originating from the *Hinf*I/*Rsa*I restriction site(s) to the origin of telomeric repeats. This length of DNA is calculated from a graph of individual T/S ratios (x-axis) plotted against the TRFL (19). The y-intercept of the regression line describing the T/S vs TRFL plot estimates the difference (in kb) of the (relative) telomeric length (obtained by RT–PCR) and the TRFL, that is, the subtelomeric DNA segment. Values are given as the y-intercept when $x = 0.0$ (mean ± 95% confidence interval).

Single-Stranded Telomere Overhang (SSTO) Length Measurements

SSTOs were isolated and their length directly measured following hybridization to a C-rich ^{32}P-labeled telomeric probe as described previously (21). DNA (5 μg) in gp32 binding buffer (10 mmol/L HEPES [pH 7.5], 30 μmol/L 2-mercaptoethanol, 100 mmol/L LiCl, 2.5 mmol/L $MgCl_2$, and 5 mmol/L $CaCl_2$) were incubated with 12 pmol/μl T4 gene 32 protein (Roche Diagnostics) and 0.2 μg/μl GST-UP1 for 1 hour at 37°C. Samples were then cross-linked with glutaraldehyde (0.02%) for 15 minutes and the reaction was stopped with 1 mol/L Tris (final concentration 30 mmol/L, pH 7.5). Double-stranded DNA was then digested with 0.04 U DNase I (Roche Diagnostics) for 30 minutes at 37°C and DNase was inactivated by treatment at 80°C for 30 minutes. SSTO DNA was obtained following overnight treatment at 55°C in the presence of 0.55 μg/μl Proteinase K (Invitrogen) and 0.5% SDS. DNA was hybridized (22°C for 16 h) to 5 fmol high-specific activity ^{32}P-C-rich probe $(CCCTAA)_3$. SSTOs were detected on 6% polyacrylamide gels (300 V for 90 min, 4°C) after drying gels on nylon membranes (Hybond+, GE Healthcare) and exposing the membranes for 16 hours (see Figure 7 for example). Images were scanned on a Typhoon 9410 VM Imager (GE Healthcare) and volume analysis of smears with in-gel calibration standards was accomplished using ImageQuant v. 5.2. Standards were run in triplicate and included 0.05 to 0.5 nmol/μl $(TTAGGG)_n$ oligomers in which n repeats were 6, 9, 16, 32, 48, or 64. Two aliquots of standard were ''unprotected,'' in that they were incubated with ^{32}P-C rich probe for 8 hours prior to electrophoresis, whereas one aliquot was ''protected'' by treatment with gp32/UP1 prior to undergoing DNase I treatment. Nonspecific ^{32}P binding for each sample (obtained by processing 5 μg DNA as above but preceded by treatment with 15 U Exonuclease I [GE Healthcare] for 16 hours at 37°C) was subtracted from each gp32/UP1-protected DNA sample prior to SSTO length calculation. The average length of the SSTO was calculated for a range of 50 to ~550 nt using a modified version of the Excel TELORUN program (21).

Telomerase Activity Measurements

Telomerase activity in cell homogenates was detected with a PCR-based telomerase detection method (telomeric repeat amplification protocol [TRAP]). Both the TRAPeze (nonisotopic gel detection) and TRAPeze XL telomerase detection (fluorescence based detection) kits (Cat #S7700 and S7707, Millipore Corp, Billerica, MA) were used. Pulverized tissues from humans or monkeys were suspended and homogenized in CHAPS lysis buffer (10 mmol/L Tris, 1 mmol/L $MgCl_2$, 1 mmol/L EGTA, 0.1 mmol/L benzamidine, 5 mmol/L β-mercaptoethanol, 0.5% CHAPS, and 10% glycerol, pH 7.5), incubated on ice for 30 minutes, and centrifuged at $12{,}000 \times g$ for 20 minutes at 4°C. Protein concentration was determined with the Bio-Rad Protein determination assay (Bio-Rad Laboratories, Hercules, CA), using bovine serum albumin as standard, and supernatant stored at −80°C. For assays, 2.5 μg protein extract was incubated in a reaction mixture containing 20 mmol/L Tris, 1.5 mmol/L $MgCl_2$, 63 mmol/L KCl, 0.05% Tween 20, and 1 mmol/L EGTA, pH 8.3) in a 24-well PCR microplate for 30 minutes at 30°C. Endogenous telomerase enzyme was inactivated for 5 minutes at 90°C, and telomerase-generated products were amplified in a PE 2400 thermal cycler using 32 cycles (59°C at 30 s, and 94°C at 30 s). Products were visualized on a 10% nondenaturing polyacrylamide gel after staining with SYBR Green I. Positive controls (C293 cells, 250 cells/rxn) and primer/dimer template controls were run for every reaction. The presence and extent of ladder formation (at 6 bp intervals) was recorded for each tissue.

Human kidney (medulla and cortex) and lung tissues were negative for telomerase activity (cf. 22, data not shown), similar to macaque renal, lung, skeletal, skin, pancreas, and adipose tissues. However, several monkey tissues did exhibit telomerase activities and were further analyzed with the semiquantitative TRAPeze XL kit. Next, 50 μl PCR reactions in 96-well plates were performed per manufacturer's recommendations on an ABI 7700 (Applied Biosystems, Foster City, CA). TaKaRa Taq polymerase was from Takara Mirus Bio, Otsu, Japan. Homogenates of tissue extracts (1 μg) and TSR8 standards, minus-DNA, heat-treated extracts (90°C for 10 min) and minus-Taq controls were run in duplicate. In this assay, fluorescent emission products generated through endogenous telomerase activities (detected through Sybr Green) were compared to the amplification of an internal control template (TSK2, detected through sulphorhodamine). Next, 40 μl of PCR reaction were diluted 1:30 in 150 mmol/L NaCl and Sybr Green I and sulphorhodamine fluorescence recorded using a SPEX spectrofluorimeter (excitation/emission wavelengths of 495/516 and 600/620). Data are expressed in Total Product Generated (TPG) units, in which 1 TPG unit

Table 1. Mean TRFLs for Male and Female Macaque Tissues and Organs

	Age* (y)	Arm Bicep	Pectoralis Major	Gluteus Maximus	Gastroc-nemius	Kidney Cortex	Kidney Medulla	Skin	Spleen	Thyroid	Pancreas	Lung	Abdominal Fat	Testis
Males														
Mean	12.2	16.3	16.2	15.6	17.0	16.2	16.4	15.5	17.2	17.9	16.2	17.0	16.3	17.5
SD	7.8	1.4	1.3	1.3	1.8	0.9	1.4	1.4	1.2	1.6	1.7	2.2	1.5	0.9
N	12	11	11	11	10	10	11	10	11	6	11	9	11	9
														Ovary
Females														
Mean	17.1	16.6	16.2	17.2	16.6	17.1	16.5	15.3	16.4	17.2	16.4	15.7	16.1	17.4
SD	7.8	1.7	1.4	2.4	1.4	1.8	1.4	2.3	1.5	2.1	2.6	1.7	2.0	1.6
N	11	10	9	9	10	9	10	10	9	7	10	9	9	7

Notes: *Approximate age (age of older monkeys is estimated).
TRFL = terminal restriction fragment length; *SD* = standard deviation.

corresponds to 1 fmole of TSR8 standard. The assay was linear from 2–500 TPG units ($r^2 > 0.99$).

Statistical Analysis

Data are expressed as mean ± standard error (*SEM*) except for Table 1 (mean ± *SD*); the number of tissues analyzed is indicated in parentheses. General linear models were used to evaluate the effect of organ differences, age (young vs mature), and sex on TRF lengths and differences in TRF lengths. Mixed models were used to accommodate repeated measures on the same monkey or human.

Analysis of covariance was used to calculate means, *SE*, and differences in y-intercept values for TRF/T/S ratios. Student's *t* test was used for SSTO lengths. For telomerase activities in individual tissues, TPG data was first transformed to ranks, and the Student-Newman-Keuls test (SNK) within analysis of variance (ANOVA) was used to evaluate relative level of telomerase tissue activity. Results with *p* values less than .05 were considered statistically significant, *p* values less than .1 were considered suggestive. SAS (v. 9.0) and GraphPad Prism (v. 4.02) were used.

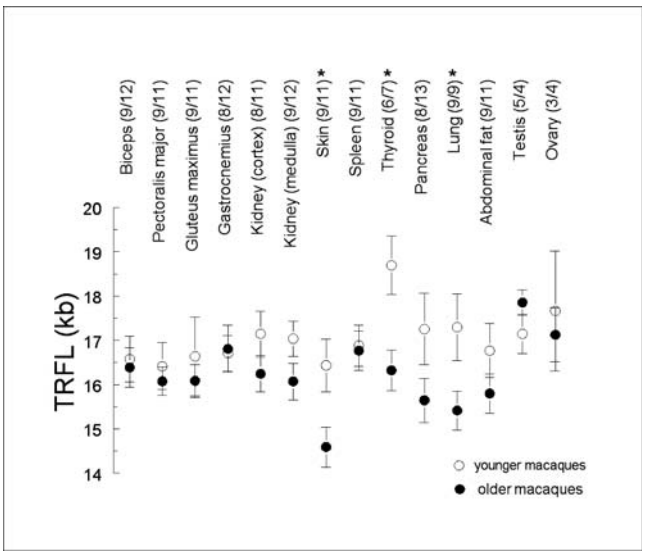

Figure 1. Terminal restriction fragment lengths (TRFLs) in younger and older macaques. Skeletal muscles and tissues were processed for telomere length determination; symbols represent the mean of younger (age 4–8 y, ○) and older (age 17–23 y, ●) animals (number of tissues analyzed for younger/older monkeys in parentheses). An * denotes statistically significant difference in organ TRFL between younger and older animals.

Results

TRFL in Macaques and Humans

Figure 1 and Table 1 display TRFLs for skeletal muscles, gonads, and various organs of the macaque. There were substantial variations in mean TRFL among animals (Table 1). Mean TRFLs varied from tissue to tissue, ranging from 15.4 kb (skin) to 17.5 kb (testis) ($p = .016$, Figure 1). These variations were observed for both younger and older animals. Skeletal muscle showed consistency among the four muscles sampled. There were no differences in the TRFL between male and female monkeys ($p > .8$).

In organ-specific analyses, significant differences were observed in the mean TRFL between younger and older animals: skin ($p = .022$), lung ($p = .046$), and thyroid ($p = .012$) tissues (Figure 1). Repeated analyses of mean TRFL of all organs (excluding ovary and testis) confirmed the age difference in skin, lung, and thyroid, as well as significant differences among organs ($p = .014$). A significant age–organ interaction ($p = .016$) indicates that age differences were not consistent across organs.

As skeletal muscle is postmitotic, we anticipated that its telomere length would not change with the donor age, reflecting telomere length at birth. Tissues in which cells do divide should exhibit decreased telomere length if compared to skeletal muscle. This concept is illustrated in Figure 2 for skeletal muscles (biceps or serratus), lung, and skin tissues from macaques and humans. Within older macaques, nonskeletal tissues had a shorter TRFL than that of the skeletal tissue ($p = .0167$ for lung vs biceps and $p = .0038$ for skin vs biceps, Figure 2A). The same relation was observed for adult humans ($p < .0001$ for lung or skin vs serratus; Figure 2B).

Telomere length in various organs from humans has been reported to exhibit congruence during intrauterine life (18,23) and partial synchrony during extrauterine life (24,25). The data displayed in Figure 2 underscore the synchronous nature of telomere length among tissues within subjects, so that an individual endowed with relatively long (or short) telomeres in one tissue tends to have relatively long

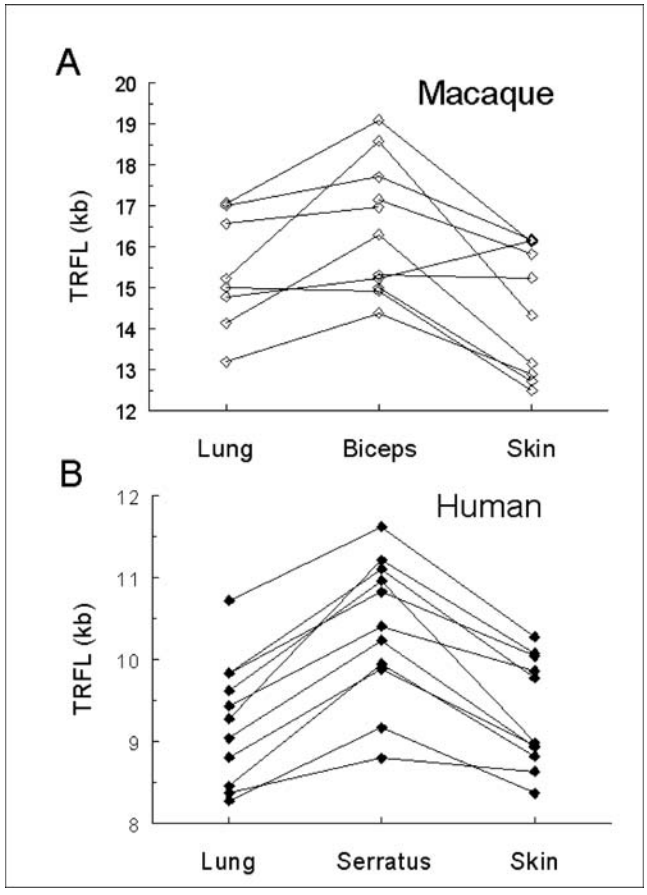

Figure 2. Terminal restriction fragment lengths (TRFLs) are longer in skeletal muscles compared to lung and skin. (**A**) Lung, biceps, and skin biopsies from older macaques were processed for TRFL determination; DNA from lung and skin tissues had significantly shorter TRFLs than DNA from the monkey's skeletal muscle. (**B**) Human lung, serratus (skeletal muscle), and skin biopsies were obtained as described in Methods and processed for telomere length determinations. In all cases, nonskeletal tissues from the same individual had shorter TRFLs than the skeletal tissue from the same subject.

(or short) telomeres in other tissues, irrespective of the replicative history of the tissues. Indeed, the effect of the individual monkey or human on mean TRFL is greater than the effect of organ differences: partial R^2s for organ and monkey are 0.23 and 0.62 (Figure 2A), and partial R^2s for organ and human are 0.43 and 0.50, respectively (Figure 2B). Further support for this proposition is shown in Figure 3, which depicts the relation between TRFL of two highly proliferating tissues, namely, lung and skin, obtained for human donors over a wide age range (newborns to 76 years). The TRFLs are from donors depicted in Figure 2B and from autopsies. The figure underscores the partial synchrony in TRFL between these highly proliferative tissues.

To test for age-related decreases in TRFL in proliferating tissues, we examined the difference (Δ) in TRFL between proliferating tissues and a reference skeletal muscle (biceps) for each monkey (Figure 4). This approach easily differentiated the ΔTRFL of older from younger animals, showing organ ($p = .0018$) and age-dependent ($p = .033$) effects

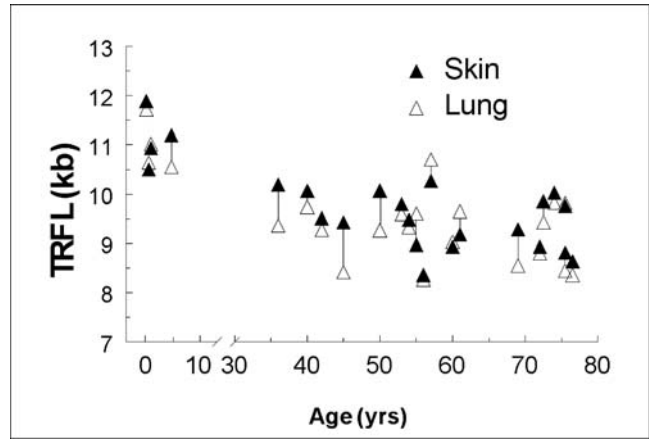

Figure 3. Partial synchrony of terminal restriction fragment length (TRFL) in human lung and skin. TRFL was measured for skin (▲) and lung (△) from 23 individuals. Note axis break at 10–30 years. The data show the partial synchrony (equivalence) in TRFL in tissues from individuals aged 0–76 years. The data are not meant to demonstrate age-dependent telomere attrition, which would require a considerably larger cohort (40).

without interaction between the two factors ($p = .24$). Significant telomere shortening in older macaques was demonstrated by the ΔTRFL for lung ($p = .0108$), pancreas ($p = .0156$), skin ($p = .0180$), and thyroid ($p = .0347$) tissues, but not in fat, spleen, or renal tissues. Thus, TRFL

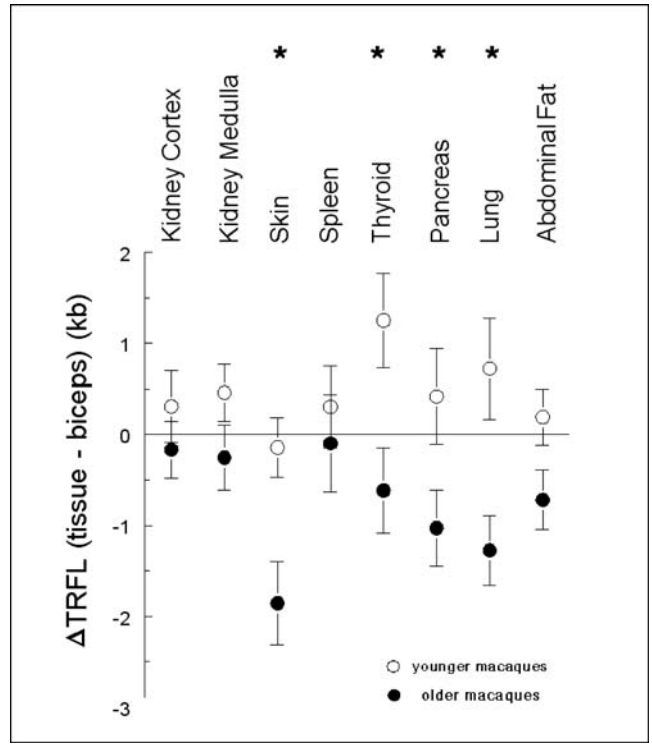

Figure 4. Δ (delta) terminal restriction fragment length (TRFL) in macaques: tissue TRFL was subtracted from the respective animal's biceps TRFL. Data are means of 6–12 tissues from younger (○) and older (●) animals. An * denotes statistically significant difference in organ TRFL between younger and older monkeys.

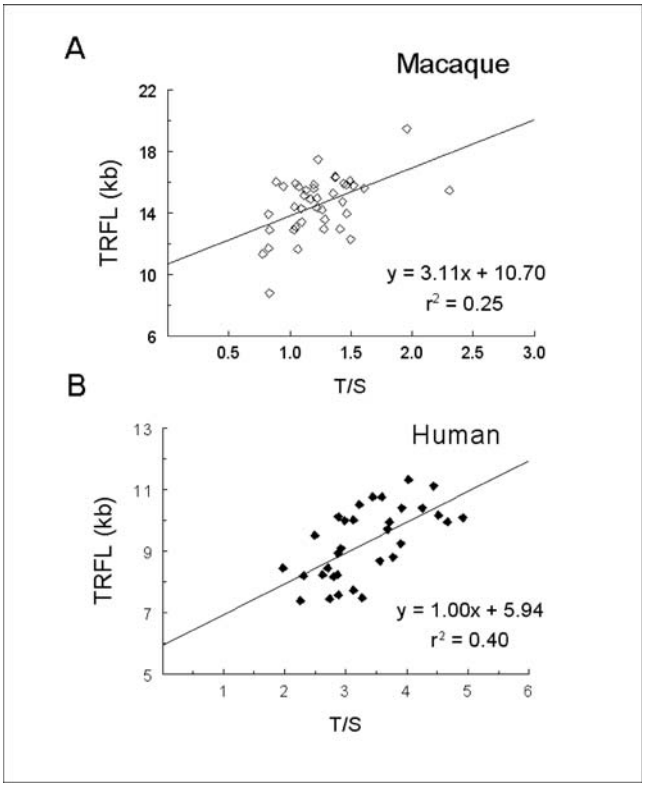

Figure 5. Subtelomeric DNA content in macaques and humans. (**A**) Subtelomeric DNA content in the macaque was assessed using real-time–polymerase chain reaction (RT–PCR) to obtain T/S ratios (telomere/single-copy ratios, utilizing *MMFPR1* as a reference gene) from 13 monkeys (2–5 tissues per monkey, $n = 40$). T/S value is plotted against the terminal restriction fragment length (TRFL) measured for the same DNA sample. DNA was from biceps, kidney medulla, skin, lung, pancreas, or spleen. The linear regression of the T/S–TRFL relation and its extrapolation to the y-axis are shown. (**B**) Subtelomeric DNA content in humans was assessed using RT–PCR; symbols represent T/S ratios (using *36B4* as the reference gene) obtained for human renal samples ($n = 32$) graphed against the respective TRFL value.

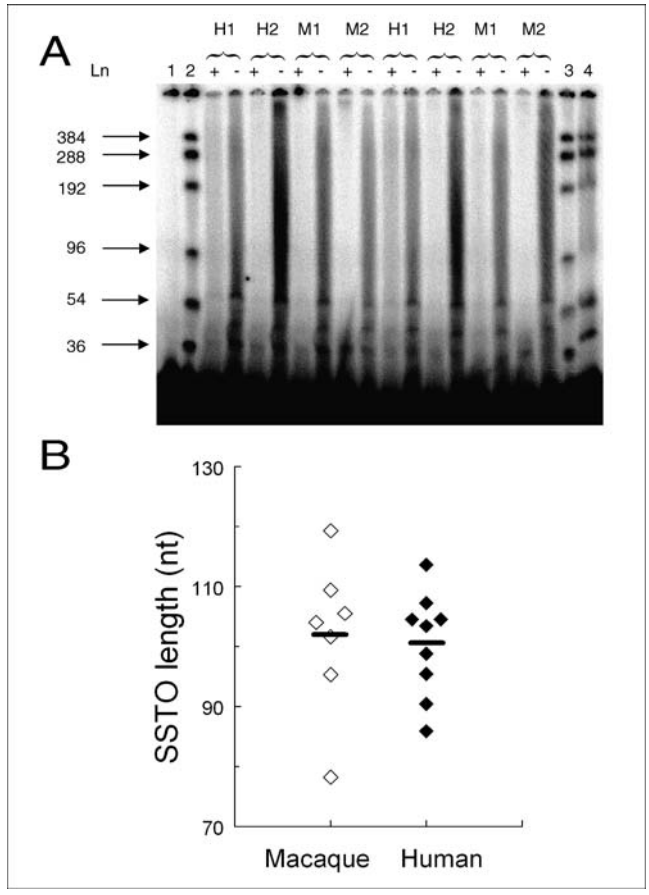

Figure 6. Single-stranded telomere overhang lengths in macaques and humans. (**A**) 5 μg DNA were processed for single-stranded telomere overhang (SSTO) length determination and electrophoresed on 6% polyacrylamide gels. Densitometric scans of SSTO in lanes indicated with a (–) were corrected for nonspecific binding (5 μg DNA treated with Exonuclease I prior to SSTO processing, as shown in lane indicated with a [+]), and the weighted mean average of single-stranded telomere signal was calculated. Calibration standards (36–384 nt of TTAGGG repeats) were included (lanes 2 and 3), as were blank (gp32 buffer containing the ^{32}P-C rich probe [lane 1]) and ''protected'' calibration standard (lane 4). The representative gel shows two human (H1, H2) and two macaque (M1, M2) samples run in duplicate (cf. left half and right half of gel). Ages of donors were: H1, 0.17 years; H2, 0.27 years; M1, 5.1 years; M2, 5.8 years. (**B**) SSTO length of macaques (◇) and humans (◆), the solid bar (—) represents the mean overhang length for each set of determinations.

analysis that incorporates a skeletal muscle reference can distinguish age-dependent shortening in specific proliferating tissues from macaques.

Telomeric and Subtelomeric Components of TRFL in Macaques and Humans

We estimated relative telomere length and the subtelomeric DNA segment in the macaque by regressing the TRFL (which measures the size of the telomeric repeats plus the digestion-resistant subtelomeric region) on the T/S ratio (using RT–PCR, which only measures the actual telomeric repeats) from the same DNA samples (Figure 5). The y-intercept represents the subtelomeric DNA length. For comparison with humans, we used human renal samples. In the macaque, the regression line extrapolated to the y-axis intercept of 10.7 ± 0.9 kb (Figure 5A). This value is significantly greater than the corresponding intercept for human tissues (5.9 ± 1.5, $p = .002$, Figure 5B). Thus, the subtelomeric DNA segment is 2.5–7.5 kb longer in macaques than in humans.

(SSTO) Length in Macaques and Humans

Telomere SSTO length was measured in kidney DNA from 7 macaques and 9 humans. Figure 6A illustrates the method for measuring overhang lengths in human and macaque samples by comparing DNA migration to a set of in-gel calibration standards. Figure 6B shows that the weighted mean average overhang length in macaques ranged from 78.2 to 119.3 nt (mean SSTO = 101.9 ± 4.8 nt) and was not different from humans (range 85.9 to 113.6 nt, mean SSTO = 100.4 ± 2.9 nt, $p = .78$).

Telomerase Activity in Macaques

We assessed telomerase activity in tissue homogenates using a PCR/gel-based detection assay. Gastrointestinal, reproductive, and hematopoietic tissues exhibited telomerase

activity, whereas skeletal and cardiac muscles, fat, and skin showed no activity (data not shown). To further characterize telomerase activity in telomerase-positive tissues, we used a semiquantitative PCR/fluorescence-based assay. Figure 7 shows the TPG of extracts from telomerase positive tissues of the macaque. Testis and thymus had the greatest activities, and spleen and stomach had greater activities than duodenum, ovary, and colon (SNK, $p < .05$, ANOVA on ranks).

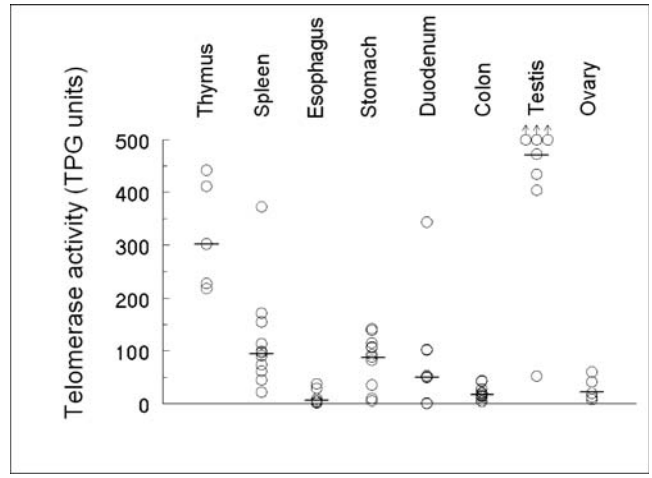

Figure 7. Telomerase activities in macaque tissues. Tissues demonstrating telomerase activity based on polymerase chain reaction (PCR)/gel analysis were semiquantitatively assessed for telomerase activities using a fluorescence-based dye PCR strategy (see Methods). 1 TPG (Total Product Generated) unit corresponds to 1 fmole of TSR8 standard. The solid bar (—) represents the median TPG for each tissue. (⍜) indicates TPG activity greater than 500 units.

Discussion

The present study demonstrates several features of telomere biology in the macaque. First, the TRFL is longer in macaques than in humans. Second, telomeres undergo attrition with advancing age in some proliferating tissues, but with little evidence for telomere erosion in postmitotic tissues such as skeletal muscle. This fact may be used to gauge age-dependent telomere erosion in the macaque, using skeletal tissue as an internal telomeric reference. Third, telomere length demonstrates partial synchrony within tissues of the macaque. Fourth, the subtelomeric DNA segment is significantly longer in macaques than in humans. Fifth, the length of the single-strand telomere overhang is similar between the two species. Lastly, we confirmed that the distribution of telomerase activity in macaque tissues resembles that of human tissues (26).

The first conclusion of this study is this: Given that both the TRFL and the subtelomeric DNA segment are longer in macaques than in humans, the difference in real telomere length between the two species is considerably smaller than that defined by TRFL analysis alone. The second conclusion is that the TRFL variation among macaques is as wide as in humans. The assessment of age-related differences in TRFLs by cross-sectional analysis in humans has traditionally required large numbers of subjects due to the interindividual variation in TRFL at birth and thereafter. For obvious reasons, such an approach is hardly applicable to nonhuman primates, the numbers of which are rather limited in laboratory studies. To overcome the effect of the interanimal variation in TRFL, we exploited the apparent constancy of skeletal muscle TRFL throughout life. We utilized this fact to distinguish telomere length of proliferating tissues between younger and older animals.

The knocking out of telomerase in the mouse causes dramatic shortening of telomere length across generations, premature aging, and diminished life span in late generations (13–15). However, the information gained from these models may be only partially applicable to humans due to the following reasons. During extrauterine life, mice demonstrate considerable telomerase activity in most somatic tissues, while humans and macaques have only modest telomerase activity, which is restricted to specific somatic tissues, for example, the alimentary tract, thymus, and endometrium (26–29). In addition, rodents have a short life span and most have relatively long telomeres (27,30,31). Thus, mean telomere length in the soma of most rodents may be neither a reliable index of the history of cell replication nor a determinant in life span. From this perspective, the telomerase knock-out mouse (11,31), for instance, is not strictly a model of aging but of diseases such as dyskeratosis congenita (32).

Thus the question is whether charting telomere dynamics in the macaque will be helpful in understanding the biology of its aging. Human data (primarily based on cross-sectional analysis) suggest that age-related disorders, including adult obesity, atherosclerosis, and essential hypertension are associated with shortened TRFL (5–12,33). However, these studies have provided mainly associative data, based primarily on telomere dynamics in leukocytes.

Here is where the nonhuman primate model will be helpful, as it may enable exploring telomere dynamics in multiple tissues in various experimentally induced states analogous to human diseases and conditions. As telomere attrition has been linked to factors such as oxidative stress in cultured cells (34) and oxidative stress and inflammation in humans (3,9–12,35), the nonhuman primate may also serve to examine how systemic oxidative stress/inflammation may affect telomere attrition, not only in leukocytes but also in other proliferating cells.

It is still uncertain, however, whether the nonhuman primate will be a useful model to explore a causal relation between telomeres and life span. Recent studies with aging baboons suggests that telomeres undergo attrition in circulating blood cells (36), and increased telomere dysfunction in dermal fibroblasts is associated with other markers of cellular senescence (37). Based on tissue culture studies, it is not the mean telomere length but the length of the shortest telomeres that ultimately triggers the growth arrest of cultured somatic cells (38,39). Given that humans live longer and possess shorter telomeres than other primates, it is possible that a subset of telomeres with short length rather than the mean telomere length is a central player in the life span of humans, nonhuman primates, and perhaps other species.

Acknowledgments

Supported by National Institutes of Health grants AG021593 and AG020132, The Healthcare Foundation of New Jersey (A.A.), Lung Cancer SPORE p50 CA75907, and NSCOR NNJ05HD36G (J.W.S.).

Current addresses: Dr. Chai: Department of Biology, Texas Woman's University, Denton, TX 76204; Dr. Durrani: Susquehanna Health System, Williamsport Hospital, Department of Pulmonary and Critical Care Medicine, Williamsport, PA 17701; Dr. Tchakmakjian: Stamford Hospital, 30 Shelburne Rd., Stamford, CT 06904.

Correspondence

Address correspondence to Jeffrey P. Gardner, PhD, The Center of Human Development and Aging, Room F-464, MSB, University of Medicine and Dentistry of New Jersey, New Jersey Medical School, 185 South Orange Ave., Newark, NJ 07103. E-mail: gardner@umdnj.edu

References

1. Aviv A. Telomeres and human aging: facts and fibs. *Sci Aging Knowledge Environ.* 2004;2004(51):pe43.
2. Wu X, Amos CI, Zhu Y, et al. Telomere dysfunction: a potential cancer predisposition factor. *J Natl Cancer Inst.* 2003;95:1211–1218.
3. von Zglinicki T, Serra V, Lorenz M, et al. Short telomeres in patients with vascular dementia: an indicator of low antioxidative capacity and a possible risk factor? *Lab Invest.* 2000;80:1739–1747.
4. Jeanclos E, Krolewski A, Skurnick J, et al. Shortened telomere length in white blood cells of patients with IDDM. *Diabetes.* 1998;47:482–486.
5. Benetos A, Okuda K, Lajemi M, et al. Telomere length as an indicator of biological aging: the gender effect and relation with pulse pressure and pulse wave velocity. *Hypertension.* 2001;37(2 Part 2):381–385.
6. Benetos A, Gardner JP, Zureik M, et al. Short telomeres are associated with increased carotid atherosclerosis in hypertensive subjects. *Hypertension.* 2004;43:182–185.
7. Samani NJ, Boultby R, Butler R, Thompson JR, Goodall AH. Telomere shortening in atherosclerosis. *Lancet.* 2001;358:472–473.
8. Cawthon RM, Smith KR, O'Brien E, Sivatchenko A, Kerber RA. Association between telomere length in blood and mortality in people aged 60 years or older. *Lancet.* 2003;361:393–395.
9. Epel ES, Blackburn EH, Lin J, et al. Accelerated telomere shortening in response to life stress. *Proc Natl Acad Sci USA.* 2004;101: 17312–17315.
10. Demissie S, Levy D, Benjamin EJ, et al. Insulin resistance, oxidative stress, hypertension, and leukocyte telomere length in men from the Framingham Heart Study. *Aging Cell.* 2006;5:325–330.
11. Aviv A, Valdes A, Gardner JP, Swaminathan R, Kimura M, Spector TD. Menopause modifies the association of leukocyte telomere length with insulin resistance and inflammation. *J Clin. Endocrinol Metab.* 2006;91:635–640.
12. Fitzpatrick AL, Kronmal RA, Gardner JP, et al. Leukocyte telomere length and cardiovascular disease in the Cardiovascular Health Study. *Am J Epidemiol.* 2007 Jan 1;165(1):14–21. Epub 2006 Oct 16.
13. Lee HW, Blasco MA, Gottlieb GJ, Horner JW 2nd, Greider CW, DePinho RA. Essential role of mouse telomerase in highly proliferative organs. *Nature.* 1998;392:569–574.
14. Rudolph KL, Chang S, Lee HW, et al. Longevity, stress response, and cancer in aging telomerase-deficient mice. *Cell.* 1999;96:701–712.
15. Espejel S, Klatt P, Menissier-de Murcia J, et al. Impact of telomerase ablation on organismal viability, aging, and tumorigenesis in mice lacking the DNA repair proteins PARP-1, Ku86, or DNA-PKcs. *J Cell Biol.* 2004;167:627–638.
16. Kakuo S, Asaoka K, Ide T. Human is a unique species among primates in terms of telomere length. *Biochem Biophys Res Commun.* 1999;263: 308–314.
17. Steinert S, White DM, Zou Y, Shay JW, Wright WE. Telomere biology and cellular aging in nonhuman primate cells. *Exp Cell Res.* 2002;272:146–152.
18. Okuda K, Bardeguez A, Gardner JP, et al. Telomere length in the newborn. *Pediatr Res.* 2002;52:377–381.
19. Cawthon RM. Telomere measurement by quantitative PCR. *Nucleic Acids Res.* 2002;30(10):e47.
20. Alvarez V, Coto E, Setien F, Gonzalez-Roces S, Lopez-Larrea C. Molecular evolution of the N-formyl peptide and C5a receptors in non-human primates. *Immunogenetics.* 1996;44:446–452.
21. Chai W, Shay JW, Wright WE. Human telomeres maintain their overhang length at senescence. *Mol Cell Biol.* 2005;25:2158–2168.
22. Tchakmakjian L, Gardner JP, Wilson PD, et al. Age-dependent telomere attrition as an indicator of racial differences in renal growth patterns. *Nephron Exp Nephrol.* 2004;98(3):e82–88.
23. Youngren K, Jeanclos E, Aviv H, et al. Synchrony in telomere length of the human fetus. *Hum Genet.* 1998;102:640–643.
24. Martens UM, Zijlmans JM, Poon SS, et al. Short telomeres on human chromosome 17p. *Nat Genet.* 1998;18:76–80.
25. Butler MG, Tilburt J, DeVries A, Muralidhar B, Aue G, Hedges L, Atkinson J, Schwartz H. Comparison of chromosome telomere integrity in multiple tissues from subjects at different ages. *Cancer Genet Cytogenet.* 1998;105:138–144.
26. Kim NW, Piatyszek MA, Prowse KR, et al. Specific association of human telomerase activity with immortal cells and cancer. *Science.* 1994;266:2011–2015.
27. Prowse KR, Greider CW. Developmental and tissue-specific regulation of mouse telomerase and telomere length. *Proc Natl Acad Sci U S A.* 1995;92:4818–4822.
28. Chadeneau C, Siegel P, Harley CB, Muller WJ, Bacchetti S. Telomerase activity in normal and malignant murine tissues. *Oncogene.* 1995;11:893–888.
29. Wright WE, Piatyszek MA, Rainey WE, Byrd W, Shay JW. Telomerase activity in human germline and embryonic tissues and cells. *Dev Genet.* 1996;18:173–179.
30. Kipling D, Cooke HJ. Hypervariable ultra-long telomeres in mice. *Nature.* 1990;347:400–402.
31. Blasco MA, Lee HW, Hande MP, et al. Telomere shortening and tumor formation by mouse cells lacking telomerase RNA. *Cell.* 1997;91: 25–34.
32. Vulliamy T, Marrone A, Szydlo R, Walne A, Mason PJ, Dokal I. Disease anticipation is associated with progressive telomere shortening in families with dyskeratosis congenita due to mutations in TERC. *Nat Genet.* 2004;36:447–449.
33. Valdes AM, Andrew T, Gardner JP, et al. Obesity, cigarette smoking, and telomere length in women. *Lancet.* 2005;366:662–664.
34. von Zglinicki T, Saretzki G, Docke W, Lotze C. Mild hyperoxia shortens telomeres and inhibits proliferation of fibroblasts: a model for senescence? *Exp Cell Res.* 1995;220:186–193.
35. Epel ES, Lin J, Wilhelm FH, et al. Cell aging in relation to stress arousal and cardiovascular disease risk factors. *Psychoneuroendocrinology.* 2006;31:277–287.
36. Baerlocher GM, Mak J, Roth A, Rice KS, Lansdorp PM. Telomere shortening in leukocyte subpopulations from baboons. *J Leukoc Biol.* 2003;73:289–296.
37. Herbig U, Ferreira M, Condel L, Carey D, Sedivy JM. Cellular senescence in aging primates. *Science.* 2006;311:1257–1259.
38. Hemann MT, Strong MA, Hao LY, Greider CW. The shortest telomere, not average telomere length, is critical for cell viability and chromosome stability. *Cell.* 2001;107:67–77.
39. Zou Y, Sfeir A, Gryaznov SM, Shay JW, Wright WE. Does a sentinel or a subset of short telomeres determine replicative senescence? *Mol Biol Cell.* 2004;15:3709–3718.
40. Aviv A, Valdes AM, Spector TD. Human telomere biology: pitfalls of moving from the laboratory to epidemiology. *Int J Epidemiol.* 2006; 35:1424–1429. Epub 2006 Sep 22.

Received July 19, 2006
Accepted October 17, 2006
Decision Editor: Huber R. Warner, PhD